Biomaterials Advances 173 (2025) 214231

Contents lists available at ScienceDirect

Biomaterials Advances

journal homepage: www.journals.elsevier.com/materials-science-and-engineering-c

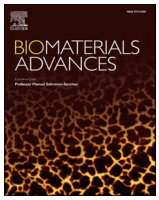

Impact of adjustable swelling dynamics on the structural integrity of sunflower pollen microgels

Snehasish Basu [a,b], Mohammed Shahrudin Bin Ibrahim [a,b], Jian Li [a,b], Jueying Yang [c], Ahmad Albar [a,b], Abdul Rahim Ferhan [a,b], Vladimir P. Zhdanov [d], Du Yeol Ryu [e], Nam-Joon Cho [a,b], Juha Song [b,f,*], Woncheol Jeong [a,b,**]

[a] School of Materials Science and Engineering, Nanyang Technological University, 50 Nanyang Avenue, 639798, Singapore
[b] Centre for Cross Economy, Nanyang Technological University, 60 Nanyang Drive, 637551, Singapore
[c] School of Materials Science and Engineering, Beijing Institute of Technology, Beijing 100081, China
[d] Boreskov Institute of Catalysis, Russian Academy of Sciences, Novosibirsk 630090, Russia
[e] Department of Chemical and Biomolecular Engineering, Yonsei University, 50 Yonsei-ro, Seodaemun-gu, Seoul 03722, South Korea
[f] School of Chemistry, Chemical Engineering and Biotechnology, Nanyang Technological University, 62 Nanyang Drive, 637459, Singapore

ARTICLE INFO

Keywords:
Sunflower pollen
Microgel
Swelling
Shell size
Potassium ions
Rheology

ABSTRACT

Pollen is a renewable biomaterial found in seed-bearing plants, and the biocompatibility of pollen microgels is a key factor driving their use in drug delivery, biosensor development, and wound care applications. Herein, the microgel was synthesized from sunflower bee pollen by using a cost-effective process, and to examine its structural integrity under adverse acidic and alkaline conditions, digital microscopy and dynamic image particle analysis were carried out. Swelling dynamics of pollen microgels were regulated by varying pH conditions, and adding aqueous KOH to the solution, and the influence of swelling-deswelling on bulk rheology and local elastic properties were experimentally investigated and theoretically interpreted by using the Ross-Minton equation for the suspension viscosity. The present findings reveal how pollen microgels can be adapted to acidic to alkaline environments in order to modify mechanical and rheological properties.

1. Introduction

Plant pollen grains play a vital role in the reproduction of flowering plants. The primary function of pollen is to fertilize the ovules (female reproductive organs) of flowers, leading to the formation of seeds [1–3]. Pollen is typically microscopic and lightweight, known as one of the most durable plant materials. It consists of an outer layer (exine) made up of cross-linked biopolymer called sporopollenin and an inner layer (intine) assembled by mainly three different polysaccharides: cellulose, pectin and hemicellulose [4–7]. Its resilience and intricate structure have been a source of inspiration for biomimetic design in various fields, from materials science to architecture [8–12]. Therefore, the intricate properties of pollen, including its mechanical strength, chemical composition, and adhesion capabilities, have already delivered different value-added products applicable in the different fields (agriculture, biotechnology and material science) by altering its native structure [9,10,13–15].

The plant intracellular pH conditions play a crucial role in pollen tube development, germination, and overall reproductive processes [16–18] and can impact the activity of enzymes [19,20], gene expression [19,21], and overall cellular processes [22,23]. The variation of pH conditions in experimental settings allows one to investigate the role of this factor in pollen physico-chemical properties. Our previous work demonstrated that certain eudicot pollen grains, such as Helianthus (sunflower), Camellia, and Baccharis, can be efficiently transformed into uniform, stimulus-responsive microgels using a simple, eco-friendly soapmaking process [24]. This transformation is highly dependent on environmental factors, including pH and ion presence [25]. Under alkaline conditions, eudicot pollen grains undergo structural modifications, softening into microgel particles due to exine layer weakening and pectin de-esterification [25]. However, this response is species-dependent—monocots, gymnosperms, and spore-bearing lycophytes exhibit distinct structural and mechanical properties that limit their responsiveness. For example, Lycopodium spores showed minimal

* Correspondence to: J. Song, Centre for Cross Economy, Nanyang Technological University, 60 Nanyang Drive, 637551, Singapore.
** Correspondence to: W. Jeong, School of Materials Science and Engineering, Nanyang Technological University, 50 Nanyang Avenue, 639798, Singapore.
E-mail addresses: songjuha@ntu.edu.sg (J. Song), woncheol.jeong@ntu.edu.sg (W. Jeong).

https://doi.org/10.1016/j.bioadv.2025.214231
Received 23 December 2024; Received in revised form 31 January 2025; Accepted 13 February 2025
Available online 15 February 2025

structural changes across pH variations, highlighting the strong material dependence of pH-responsive swelling and deswelling [25]. Sunflower pollen was chosen as the model system due to its well-characterized pH-responsive behavior, making it an ideal representative for studying swelling and rheological properties in response to chemical treatments, particularly with KOH.

Sunflower pollen microgels exhibit pH-responsive behavior, transitioning from deswelling to swelling as pH increases [25]. This indicates that the microgel particles contain pH-sensitive chemical compositions or ionic functional groups (e.g., carboxylic acid moieties) that respond to changes in protonation and deprotonation [25]. The reversible ionization of these functional groups (e.g., –COOH) generates an osmotic pressure gradient, regulating the hydration level within the gel matrix and controlling the swelling and deswelling process [25]. This property, commonly observed in "smart hydrogels," has been exploited for applications such as nano-valves to control fluid fluxes in microfluidic systems [26,27].

Pectin, identified in the intine layer of sunflower pollen, undergoes significant de-esterification during microgel preparation following KOH treatment [25]. This de-esterified pectin plays a crucial role in the pH-responsive swelling behavior of pollen microgels. The presence of carboxylic functional groups (–COOH) in the intine structure allows the microgels to undergo protonation or deprotonation depending on pH levels [25,28]. At higher pH (alkaline conditions), carboxylic acid groups become negatively charged (deprotonated), leading to electrostatic repulsion between $–COO^-$ groups and increased water uptake, resulting in microgel swelling. Conversely, at lower pH (acidic conditions), reduced electrostatic repulsion causes the microgel to shrink [25,28]. Beyond pH variations, pollen microgels also respond to external stimuli such as chelating agents (e.g., EDTA) and electrolyte concentration changes [25]. These factors influence structural integrity, swelling behavior, and gelation properties by modulating pectin-based cross-linking mechanisms within the pollen's intine layer. Understanding these responsive behaviors provides valuable insights into tailoring pollen-based materials for diverse applications, including biomedical, environmental, and soft material engineering. Particularly, pH dependent swelling dynamics can cause changes in the structural morphology and overall physical characteristics of pollen microgels. The fundamental mechanism by which pH changes influence the rheological character of microgels is, however, still unknown. Understanding the bulk rheology of pollen microgels is crucial for tailoring their properties for specific applications (e.g., drug delivery, tissue engineering, 3D printing etc.) and designing materials with desired functionalities. Therefore, the present study is focused on the effects of prolonged alkali treated pH–responsive swelling/deswelling dynamics on overall viscoelasticity of non-allergenic pollen microgels. In particular, the fundamental causes behind the structural integrity of pollen microgel are examined by varying alkali concentration (KOH) and pH conditions (acidic to alkaline).

2. Materials and methods

2.1. Materials

Sunflower (*Helianthus annuus L.*) pollen grains used in the present study were purchased from Shaanxi GTL Biotech Co. Ltd. (China). Acetone, di-ethyl ether, hydrochloric acid, glycine, potassium hydroxide and D-galacturonic acid sodium salt were procured from Merck (Singapore). CAPS [3–(cyclohexylamino)propane–1–sulfonic acid] pH 9 and 11 buffers (0.5 M) were purchased from Thermo Fisher Scientific (Singapore). Deionised (DI) water was acquired from the Milli-Q, Merck (Singapore) water purifier system.

2.2. Sunflower pollen microgel preparation

The pollen microgel suspensions were prepared in the following four steps.

Defatting: Raw sunflower bee pollen particles were defatted using acetone and di-ethyl ether as described in the previous work [25].

Cytoplasmic removal (1st KOH treatment step): Defatted pollen samples (30 g) were mixed with aqueous 10 % (*w/v*) KOH (300 mL) in a polytetrafluoroethylene (PTFE) round-bottom flask. The suspension was refluxed for 2 h at 80 °C under constant magnetic stirring at 700 rpm. The resultant suspension was filtered using nylon mesh (pore size: 30 μm) and the collected pollen samples (with size ≥30 μm) were washed using fresh 10 % (*w/v*) KOH solution until the filtrate was clear. Afterwards, final suspension was transferred to 50 mL conical centrifuge tube.

Microgel formation (2nd KOH treatment step): Sample in each tube (50 mL) was topped up to a total volume of 30 mL with fresh 10 % (w/v) KOH and vortexed at high speed for 2 min. Finally, the sample was placed in a hot plate oven at 80 °C for a specific period of time (3, 6, 12, 24 and 48 h). After successive incubation, the resulting pollen suspension was washed with de-ionised water until the pH level reached 6.8–7.0 to process different (3, 6, 12, 24 and 48 h) pollen microgels. In order to prepare 0 h pollen microgel, the first KOH treatment process (cytoplasmic removal) was applied followed by water washing until the pH level reached to 6.8–7.0.

pH equilibration: Each set of microgel sample (0, 3, 6, 12, 24 and 48 h) was equilibrated in 50 mM Glycine buffers (Glycine–HCl or Glycine–KOH) at five different pH (3, 5, 7, 9, 11), separately.

2.3. Swelling/deswelling measurements

Swelling/deswelling kinetics of 50 mM Glycine buffers-swollen microgels (0, 3, 6, 12, 24 and 48 h) at different pH (3, 5, 7, 9, 11) were studied by transferring equal volume (5 mL) of each microgel solution to a glass tube, separately. After the microgels had reached swelling equilibrium for a week under ambient conditions, the swelling volume of each set of microgel in a glass tube was determined by the swelling volume of each set of microgel in a glass tube was identified with $\pi r^2 h$, where r and h are, respectively, radius and height of the microgel solution in a glass tube.

Finally, the optical images of microgel swelling/deswelling in glass tubes were captured in a LightBox integrated with LED lights.

2.4. Inductively Coupled Plasma Mass Spectrometry (ICP-MS)

Inductively Coupled Plasma Mass Spectrometry (Model: Elan DRC-e, PerkinElmer) was used to detect the different elements (Sodium, Potassium, Calcium) present in the CAPS buffers (pH 9 and 11). The calibration of the elements was tested ranging from 0.001 ppm to 0.1 ppm.

2.5. Dynamic image particle analysis

The FlowCAM (Fluid Imaging Technologies, USA) system combining 200 μm flow cell with a 10× optical lens microscopy was used to determine the size of microgel particles in a fluid medium to investigate the effect of the prolonged KOH treatment on the morphology of the pollen microgels at the different pH conditions. Microgel solutions were primed manually into the flow cell and were analysed with a flow rate of 0.1 mL min^{-1}. Images of microgel particles that pass through the optics were automatically captured (15 images s^{-1}) and recorded. The system allows for rapid acquisition of digital images of dynamic particles, enabling measurement of microgel particle size and morphology. Visual Spreadsheet software (Fluid Imaging Technologies, USA) was used to analyze microgel particle sizes under different conditions.

For pH-dependent studies, five different pH conditions were tested: 3, 5, 7, 9, and 11. For each pH condition, 3 μL of 10 % (w/v) KOH treated pollen microgel sample (0, 3, 6, 12, 24, 48 h) was mixed thoroughly with 497 μL of the corresponding pH buffer solution, separately. After an incubation period of 60 min at room temperature, 200 μL of the pollen

suspension was considered to perform FlowCAM experiment.

2.6. Digital microscopy

For each pH condition, 3 μL of different KOH treated pollen microgel sample (0, 3, 6, 12, 24, 48 h) was mixed thoroughly with 497 μL of the corresponding pH buffer solution, separately. Later, 50 μL suspension of each microgel stock was placed onto a 24 mm × 75 mm glass slide (Corning, USA) followed by imaging was performed using an automated digital microscope (Keyence VHX-7000 N, Singapore). A 500× high magnification lens was used to capture at least five images of each sample. Images were processed using VHX-H5M software. Defatted sunflower pollen particles were equilibrated at the different pH solutions (3, 5, 7, 9, 11) considered as control specimens.

2.7. Rotational viscometry

MCR 702e multidrive rheometer with temperature control at 25 °C (Anton Paar GmbH, Austria) was used to measure the viscosity of microgel solutions (0, 3, 6, 12, 24 and 48 h of incubation) at different pH (3, 5, 7, 9, 11) by transferring equal volume (10 mL) of each microgel solution to a centrifuge tube, separately to keep the same volume fraction. Initially, 300 μL drop of pollen microgel solution was placed on the bottom flat plate, and subsequently a 25 mm diameter top flat plate (PP25) was lowered to a final gap of 1.0 mm. The viscosity of all pollen microgel was measured using a continuous ramp test at shear rates from 1 to 1000 s^{-1} obtained via steady state measurement. Data were acquired and analysed with the Anton Paar software "RheoCompass" (V1.30.1164).

2.8. Oscillatory Rheology

The rheology of the pollen microgels was tested using a MCR 702e multidrive rheometer with temperature control at 25 °C (Anton Paar GmbH, Austria). Frequency sweep of microgel solutions (0, 3, 6, 12, 24 and 48 h of incubation) at different pH (3, 5, 7, 9, 11) was studied by transferring equal volume (10 mL) of each solution to a centrifuge tube, separately to keep the same volume fraction. After loading 300 μL of solution on the bottom flat plate, 1.0 mm final gap was set between the two parallel plates. The linear viscoelastic region (LVR) was found out using a strain sweep (0.01–100 %) test with a constant angular frequency of 6.28 rad/s (1 Hz). To determine the storage (G') and loss (G'') moduli, amplitude frequency and shear strain amplitude were set to 0.1–100 rad/s and 0.1 %, respectively.

3. Results and discussion

3.1. Swelling/deswelling dynamics of microgel solutions

Sunflower pollen microgel particles swell extensively at alkaline pH conditions, but this behavior can be reversed (rapid de-swelling) at acidic pH [25]. Time-lapse optical microscopy revealed the structural alterations of a single sunflower microgel particle during swelling-deswelling under varying pH conditions (2 to 14) after a specific KOH incubation period of 6 h [25]. However, swelling dynamics of microgel particles in bulk solution have not been extensively investigated.

Therefore, a detailed analysis of the effects of prolonged KOH incubation periods and different pH on a microgel particles was conducted in the present study which examined the effect of a wide range of KOH incubation periods (0 to 48 h) and pH conditions (3 to 11) on swelling-deswelling of single and bulk microgel particles in solutions. A distinct swelling volume enhancement of pollen microgel solutions was observed with increasing pH at every KOH treatment condition (Fig. 1a-f, **Fig. S1**).

The bulk microgel particles in a glass tube showed maximum swelling volume at pH 11 after short periods (0 and 3 h) of KOH treatment (Fig. 1a and b). The Dynamic image particle analysis (DIPA) indicates that the increased size of microgel particles contributed to the overall upsurge in bulk swelling volume and demonstrated that pH 11 equilibrated particles swelled maximally (~48 μm) after 0–3 h KOH treatment (Table 1).

Increasing the incubation time in the presence of KOH resulted in a greater amount of de-esterification of pectin molecules in the plant cell wall [29]. Herein, the present findings showed that the following KOH treatments beyond 3 h (6 to 48 h), the swelling volume was maximum at pH 9 rather than pH 11 (Fig. 1c–f, **Fig. S1**). A direct correlation was found between swelling volumes and microgel particle diameters, with all microgel samples (6 to 48 h) displaying maximum diameters at pH 9 and decreased at pH 11 (Table 1). Based on the FTIR analysis, an extended KOH incubation period induced additional COOH groups in de-esterified pectin was present inside microgel [28]. This indicates that the carboxyl groups of pectin are extensively deprotonated at pH 9 and showing maximum swelling dynamics. On the other hand, at pH 11, excess K^+ ions in buffer solution (KOH in this study) decrease the repulsion between the pectin polymers by shielding the negative charges of the carboxyl groups and thereby reducing swelling [28,30].

Interestingly, the colour intensity of the microgel solutions at pH 11 was significantly higher than at the lower pH conditions (Fig. 1). Initially, colour intensity at pH 11 was very prominent during the early

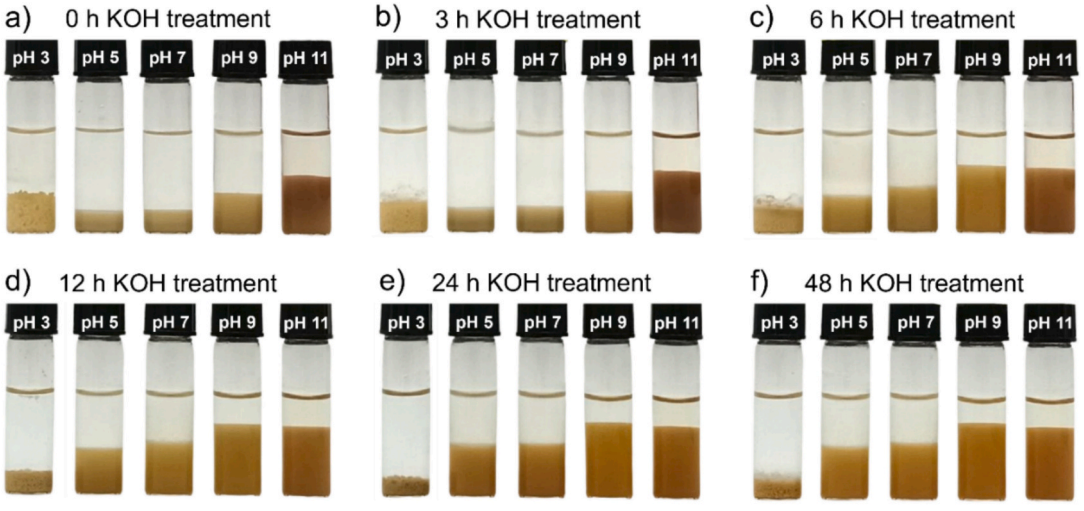

Fig. 1. Combined effect of prolonged KOH treatment durations (0–48 h) and different pH (3−11) on swelling/deswelling dynamics of pollen microgels (**a–f**).

Table 1
Average diameter of pollen microgel particles (μm) at different KOH treatment duration and pH. The underlined values correspond to the maximum diameters of microgel particles for different pollen samples.

Sample	pH 3	pH 5	pH 7	pH 9	pH 11	Diameter increment
Defatted	37.0 ± 1.7	37.0 ± 2.1	40.0 ± 2.6	40.0 ± 2.0	42.0 ± 2.1	13.5 %
0 h	33.4 ± 1.7	34.0 ± 2.1	36.0 ± 1.0	45.5 ± 2.1	48.0 ± 2.1	43.7 %
3 h	32.5 ± 1.4	34.0 ± 1.5	35.5 ± 2.3	46.5 ± 2.0	47.5 ± 2.2	46.1 %
6 h	31.9 ± 1.5	33.0 ± 2.4	35.5 ± 2.0	52.0 ± 2.3	50.3 ± 2.4	63.0 %
12 h	31.0 ± 1.3	34.0 ± 1.4	36.0 ± 2.0	55.0 ± 2.7	51.3 ± 2.2	77.4 %
24 h	29.2 ± 2.0	35.0 ± 1.8	37.0 ± 1.7	56.0 ± 3.5	51.7 ± 2.6	91.7 %
48 h	28.8 ± 1.7	34.5 ± 1.9	40.0 ± 1.9	56.5 ± 2.9	52.0 ± 2.8	96.1 %

stages of KOH treatments from 0 to 6 h and gradually decreased afterwards (Fig. 1a-f). According to the previous immunofluorescence studies, methoxy esterified pectin was present in the intine during 0–6 h of KOH treatment and completely disappeared after 12 h of KOH treatment, confirming 100 % de-esterification [25]. Due to higher amount of esterified pectin in the microgel structure, the rate of alkaline hydrolysis of ester moiety at pH 11 was boosted in 0–6 h KOH treated microgel solutions and enhanced the formation of D-galacturonic acid in the respective solutions. D-galacturonic acid was responsible for enhancing the overall colour intensity of 0–6 h KOH treated microgel solutions at pH 11 (Fig. 1a-c) as the reddish-brown colour is characteristic of D-galacturonic acid shown in the previous study [31].

To establish the hypothesis above, D-Galacturonic acid sodium salt (20 mg/mL) was equilibrated in the presence of five different pH solutions (pH 3, 5, 7, 9, 11) and kept for a week at room temperature (RT) and 80 °C, separately. RT and 80 °C conditions were considered to examine the colour changes of D-Galacturonic acid sodium salt as microgel processing was done under these two temperatures.

Under both temperatures, D-Galacturonic acid sodium salts showed brown colour at pH 11 only. The intensity of the colour was higher at the higher temperature (80 °C) as the reaction kinetics was temperature sensitive [31]. These results (Fig. 2) further revealed the higher colour intensity of the microgel solutions (0–6 h) at pH 11 condition.

The Young's modulus of the microgel's exine (outer surface) was ~600 MPa after 0 to 3 h KOH treatment and abruptly decreased to 400 MPa after 6 h treatment [25]. A further reduction was observed in the ratio between the Young's modulus of exine and intine layers from ~3 (0 and 3 h KOH treatment) to ~1.7 (6 h KOH treatment) [25]. As a result of the drastic impact on mechanical properties, the structure of the 6 h KOH treated microgel deforms significantly around its three aperture tips, allowing more K^+ influx inside the microgel and neutralizing the large number of negative charges of the carboxyl groups at pH 11, resulting in less swelling than at pH 9 (Fig. 1c). However, due to a reduction of K^+ influx inside microgel after 0–3 h KOH treatment, charge neutralization effect was significantly lower, causing elevated swelling at pH 11 (Fig. 1a and b) in the presence of greater population of free carboxylate ions in the intine. Therefore, by allowing the hydrated intine to swell more readily, a softened exine layer modulates the mechanical properties of microgel particles. It is therefore clear that the morphology of microgel particles is influenced by the interplay of mechanical responses between the outer (exine) and inner (intine) layers.

Furthermore, the most interesting phenomena were observed in 0 and 3 h KOH treated microgels equilibrated at extreme acidic condition at pH 3. Initially, swelling volumes of microgels were significantly higher at pH 3 than those at the pH 5–7 conditions (Fig. 1a and b) and this trend was completely different from that in the rest of the samples, 6–48 h (Fig. 1c–f), as pH 3 showed less swelling compared to the higher pH conditions. At low acidic condition (≈ pH 3), methoxy esterified pectin predominantly forms gels through the lateral aggregation of the neighbouring chains dominated by hydrophobic interaction and traps solvent and solute molecules within the gel network [32–36]. Previous immunofluorescence studies showed evidence regarding the presence of methoxy esterified pectin inside microgel intine layer after 0–3 h KOH treatment [25] and strongly supported higher swelling of 0 and 3 h KOH treated microgels at pH 3 condition (Fig. 1a and b).

The bulk swelling volume was reduced gradually by increasing KOH incubation from 0 to 48 h at pH 3 condition (Fig. 3a). An earlier immunofluorescence study showed that a significant amount of methoxy esterified pectin was present in the microgel intine layer after 3 h of KOH treatment, but almost disappeared after longer treatment, confirming generation of additional de-esterified pectin [25] and well supported increasing number of the protonated carboxyl group (COOH) associated to the de-esterified pectin generated in the intine layer during longer KOH treatment (6–48 h) at pH 3, causing self-aggregation through strong hydrogen bonding and reduced the swelling volume of the microgel particles (Fig. 3b). As a result of strong aggregation inside the microgel structure during 6–48 h KOH incubation, particle size (μm) regularly decreased with decreasing swelling volume (Fig. 3b), showing distinct correlation between these values.

3.2. Impact of swelling/deswelling on microgel morphology

A systematic characterization of the KOH treated microgels at each stage of processing (0–48 h) was achieved using DIPA to understand the effect of the prolonged 10 % KOH treatment at 80 °C and different pH equilibration conditions on morphological changes of the microgel particles. The corresponding results (**Fig. S2**) showed that the average size of defatted sunflower pollen spores was increased only 13 % from acidic (37 ± 1.7 μm at pH 3) to alkaline condition (42 ± 2.1 μm at pH

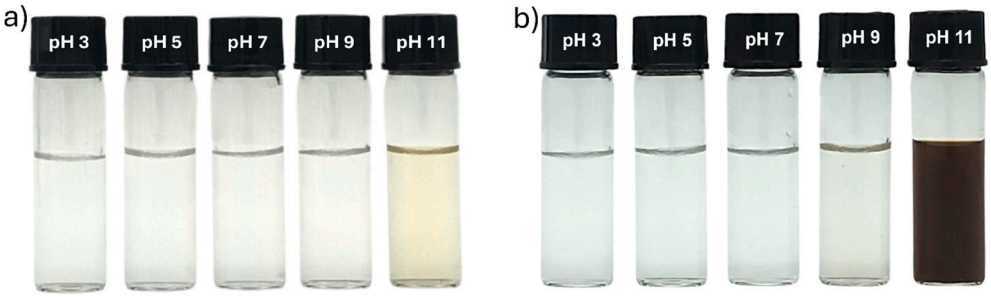

Fig. 2. Colour of D-Galacturonic acid sodium salt at room temperature (**a**) and 80 °C (**b**) at different pH conditions (3–11).

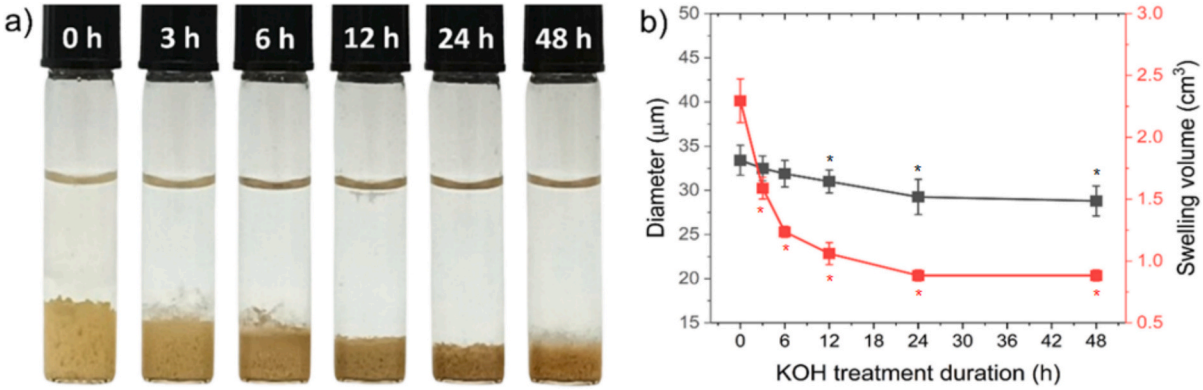

Fig. 3. Swelling/deswelling dynamics of pH 3 equilibrated microgels during prolonged KOH treatment from 0 to 48 h: (**a**) solution snapshots and **(b)** the swelling volume and particle diameter of the equilibrated microgels. The diameter (µm) was measured using Dynamic image particle analysis (DIPA). Error bars represent standard deviations ($n = 3$) and ($n = 500$) of swelling volume and diameter plots, respectively ('n' is the number of replication) The statistical analysis using Tukey's test was performed pairwise, comparing the diameter and swelling volume at 0 h with those at other time points (the statistically significant value was $^*p < 0.05$).

11). However, the corresponding increase was much more appreciable after prolonged KOH treatment, 0 to 48 h (Table 1). Shorter periods (0 and 3 h) of KOH incubation showed maximum size (underlined) differences at pH 11 (Table 1, Fig. 4), but during extended KOH incubation (6 to 48 h), maximum transformations (underlined) were observed at pH 9 and the percentage changes were recorded accordingly (Table 1, Fig. 4).

Pollen microgel treated with 10 % KOH for 48 h exhibited the largest increase in particle diameter from 28.8 to 56.5 µm at pH 9 (Table 1, Fig. 4). These results demonstrate that KOH incubation duration and alkaline pH have an impact on microgel morphology. As a result of strong aggregation inside the microgel structure during 6–48 h KOH incubation, particle size (µm) regularly decreased with decreasing swelling volume (Fig. 3b), showing distinct correlation between these values.

Additionally, during shorter duration of KOH treatments (0−3h), maximum microgel particle diameter was observed at pH 11 (Table 1, Fig. 4) which caused higher swelling volume (Fig. 1a and b). Previous studies showed that KOH treatment enhances de-esterification of pectin molecules [25,28], resulting in an increase of anionic carboxyl groups ($–COO^-$) in intine layer at alkaline conditions, causing repulsion between identical charged groups and maximum swelling at pH 11 which was in line with the maximum diameter (Table 1). With further increase in KOH incubation time (6 to 48 h), all samples showed maximum diameter at pH 9 and then decreased at pH 11 (Fig. 4). At pH 11, the excess K^+ ions reduced the repulsion between the negative charges of the carboxyl groups more effectively, resulting in smaller particles (Fig. 4).

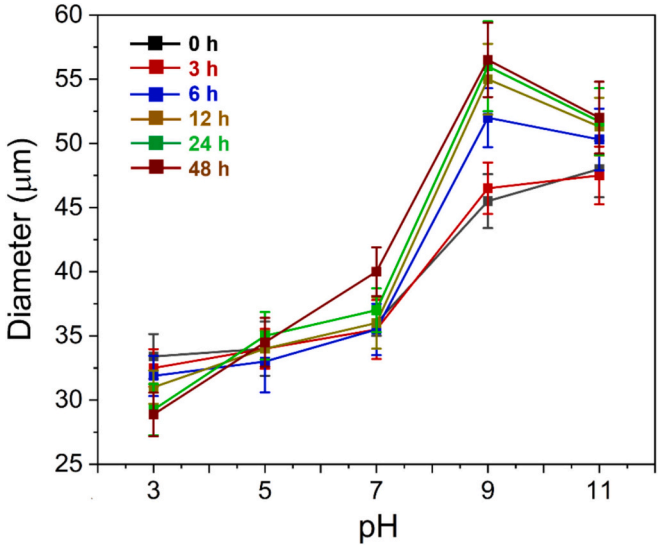

Fig. 4. Dynamic image particle analysis (DIPA) showed the influence of different pH (3–11) on the size of sunflower pollen microgel during the prolonged KOH incubation periods, 0–48 h. Error bars represent standard deviation ($n = 500$).

The effect of excess K^+ ions (Glycine–KOH buffer) on microgel swelling dynamics was further confirmed in the presence of CAPS buffers (pH 9 and 11) which contained very negligible amount of potassium element (0.0538 ppm) examined by ICP-MS technique. Also, other elements (sodium, calcium, magnesium, manganese) were present in trace amount ranging from 0.002 to 0.05 ppm. Pollen microgels were equilibrated separately with CAPS buffers at two different pH conditions (9 and 11) in the presence of very negligible amounts of K^+ ions, showed higher swelling volume at pH 11 than the pH 9 condition (Fig. 5a). The overall diameter of the CAPS pH 11 buffer equilibrated microgel particles was greater than that of the CAPS pH 9 buffer condition, resulting in an increased swelling volume (Fig. 5). Therefore, overall higher swelling volume and diameter of microgel particles in the presence of CAPS pH 11 buffer (Fig. 5) confirmed the contribution of excess K^+ ions during the equilibration by using Glycine–KOH buffer (pH 9 and 11) to microgel bulk swelling and single particle morphology.

Additionally, significant correlation between swelling volume and particle size clearly indicates that these two variables have a strong relationship (Figs. 1 and 4). Therefore, the morphological changes of the pollen microgel are controlled by the two factors; i) the concentration of deprotonated carboxyl groups influences the osmotic pressure inside the pollen microgel, which in turn affects its swelling and deswelling, and ii) the stiffness of the exine layer during extended KOH incubation determines the size of microgel particles. The digital microscopy (DM) technique was used to examine microgel particles' morphology at stationary phase (Fig. 6) in order to correlate the findings with the DIPA results as FlowCAM captured microgel images in dynamic conditions when particles moved in fluid. The digital microscopy results have also demonstrated that KOH incubation duration and alkaline pH have an impact on microgel morphology, and the trends (**Fig. S3**) were identical with the DIPA images (Fig. 4). Therefore, these two techniques, digital microscopy and DIPA images, further indicated the strong correlation between the bulk swelling volume of the microgels and their sizes.

To further characterize the change in properties of sunflower pollen microgel suspension upon being subjected to increasing duration of KOH incubation, and how these microgel suspensions react to various pH conditions, viscosity of the resultant microgel suspension was measured at defined time points (0–48 h) and subjected the respective suspensions to various pH (**Fig. S4**). As microgel suspensions at pH 3 were highly

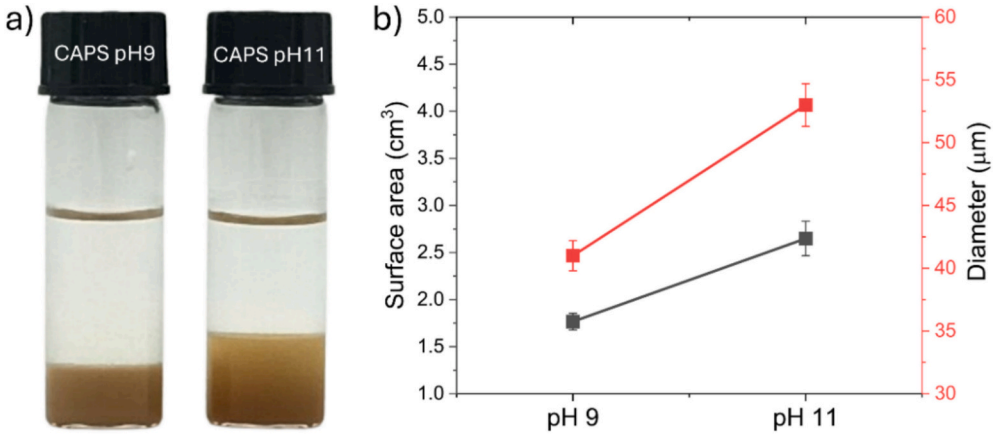

Fig. 5. Swelling/deswelling dynamics of CAPS buffer (pH 9 and 11) equilibrated 6 h KOH treated microgels in bulk solutions (**a**). Relation between the swelling volume and diameter of the CAPS buffer pH 9 and 11 equilibrated microgels (**b**). Microgel particle diameter (µm) was examined using Dynamic image particle analysis (DIPA). Error bars represent standard deviations ($n = 3$) and ($n = 500$) of swelling volume and diameter plots, respectively.

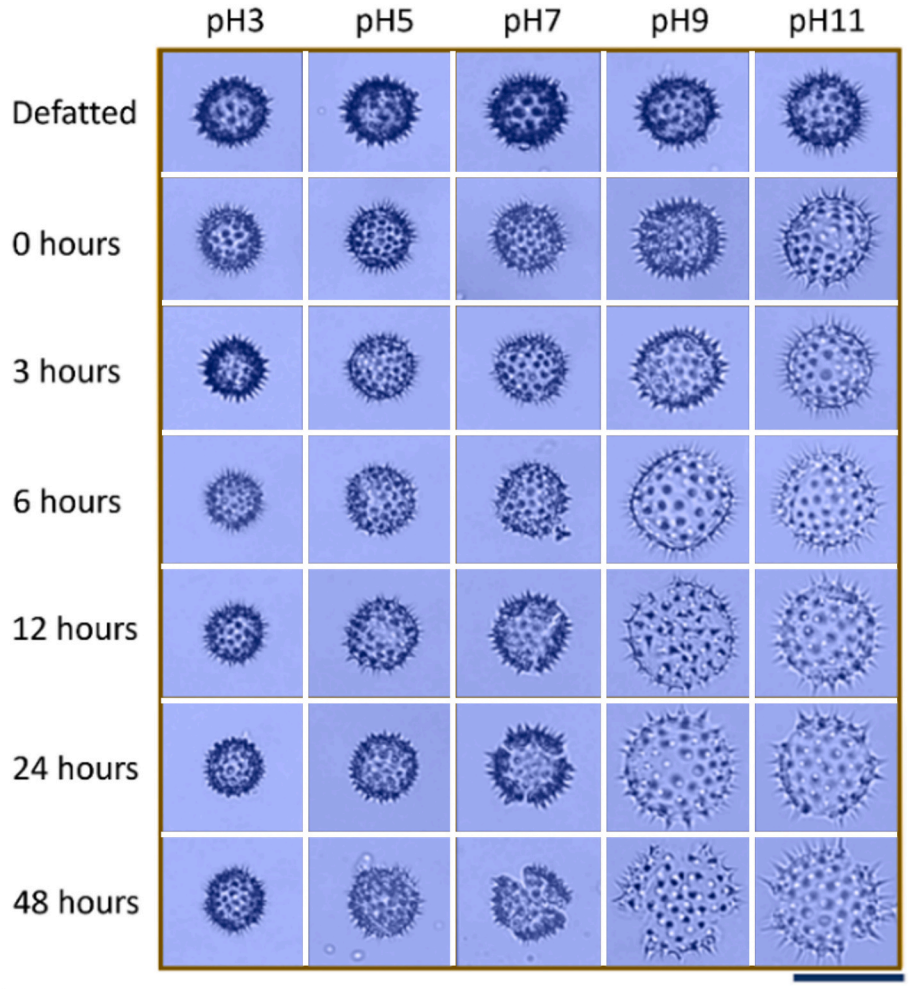

Fig. 6. Digital microscopy images explicitly demonstrate the combined effect of different pH (3–11) equilibrated sunflower pollen microgels after prolonged KOH treatment (0 to 48 h) on swelling/deswelling dynamics. Scale bar: 50 µm.

inhomogeneous due to the extensive aggregation of the particles (Fig. 1a–f), viscosity measurements of the pH 3 samples were unsuitable for comparative measurement. After incubation in 10 % KOH at 80 °C for different duration (0–48 h), pollen microgels showed maximum viscosity at 12 h, after which the viscosity dropped (Fig. 7). Also, 12 h sample consistently showed the highest viscosity in a wide range of pH conditions and reached the peak at pH 9 (Fig. 7**)**. Thus, the present study showed an increase in the size of sunflower pollen microgel particles contributed to advanced swelling, which ultimately increases the viscosity under alkaline conditions. When particles swell, they absorb more

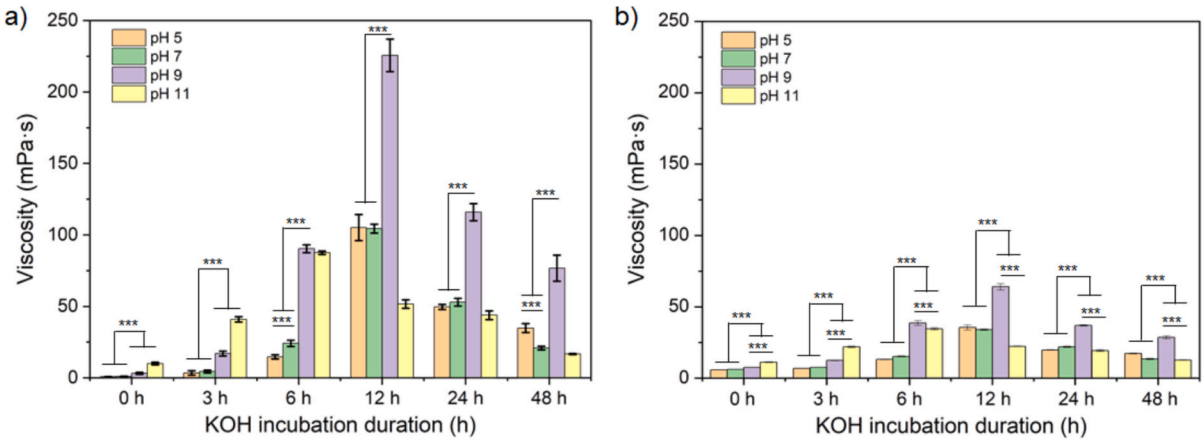

Fig. 7. Viscosity of microgels synthesized from specific KOH incubation timepoints and subjected to various pH at low, 155 s^{-1} (**a**) and high shear rate, 1000 s^{-1} (**b**). The data are grouped according to duration of KOH incubation and pH variation. Error bars represent standard deviation ($n = 3$). The statistical analysis using Tukey's test was performed pairwise, comparing the viscosity at pH 5 with that at other pH levels (***$p < 0.001$).

solvent or dispersant, causing them to increase in size. As a result, the interactions between particles become more significant, leading to a tighter packing arrangement and increased resistance to flow, causing increase in viscosity.

Additionally, 12, 24 and 48 h KOH treated microgel particles showed almost equivalent sizes at similar pH conditions (Table 1). Interestingly, despite similar particle sizes, 24 and 48 h samples displayed significant reductions in viscosity in comparison with the 12 h sample (Fig. 7). Previous study had demonstrated the reduction of the Young's modulus of the pollen microgel particle with increasing duration of KOH incubation period [25]. Therefore, the continual decrease in rigidity of the sunflower pollen microgel particle beyond 12 h was not able to withstand the high shear force during the viscosity measurement, resulting in a decrease in viscosity due to suppressed swelling. The volume fraction of the microgel polymer network in the solvent was increased during swelling, leading to a higher effective volume fraction. This increased volume fraction contributed to the overall viscosity of the microgel. However, when high shear force was applied, it disrupted the swollen state of the microgel, causing a reduction in the effective volume fraction dependent viscosity. As a result, the softer microgels were more susceptible to the effects of high shear rates. Thus, throughout prolonged alkali treatments, particularly within a 24–48 h period, the rigidity of the pollen microgel becomes the dominant factor determining the viscosity of the microgel suspension. The samples corresponding to 12 h incubation period showed peak viscosity among all microgel suspensions and were chosen below for the in-depth rheological characteristics at different pH (3–11) to determine the effects of acidic or alkaline conditions on structural integrity.

Regarding viscosity, one can add that physically pollen microgel can be classified as a special type of suspensions. The viscosities of various suspensions have long been studied experimentally and theoretically. Analytically, the accurate expression for the viscosity,

$$\eta = \eta_0[1 + (5/2)\varphi], \tag{1}$$

can be obtained (see e.g. §22 in Ref. [37]) provided the suspended particles are undeformable, and the fraction of volume, φ, is small (η_0 is the viscosity at $\varphi \to 0$). Many other expressions for the viscosity were often inspired by Eq. (1) and frequently contain additional empirically introduced factors (see e.g. Table 4 in the recent review by Rahman et al. [38]). In our context, it is instructive to recall the widely used expression proposed for suspensions of proteins by Ross and Minton [39] (for recent examples of its application, see e.g. Refs. [40, 41]),

$$\eta = \eta_o exp\left[\frac{\eta_{in} c}{1 - (k/\nu)\eta_{in} c}\right], \tag{2}$$

where η_{in} and c are the properly defined intrinsic viscosity and concentration of particles (according to [39], c is the weight concentration), and k and ν are the crowding and shape factors, respectively. In numerous studies of proteins, this expression is often employed to describe rapid increase of η with increasing c.

The use of Eqs. (1) and (2) typically implies that particles, such as proteins, are closely packed inside. In our case, however, pollen microgel particles can be viewed as hollow shells (with pores) filled with water. This raises the question of whether the internal water should be considered as trapped within the particle itself (Case 1) or as part of the surrounding solution (Case 2), as illustrated in **Fig. S7**.

In Case 1, including this internal water in the weight concentration measurement could lead to an overestimation of the pollen microgel concentration, since the total weight would encompass both the water absorbed within the hydrogel layer and the trapped internal water. To prevent this overestimation, we selected Case 2, where internal water is excluded when determining particle weight and concentration. This approach is consistent with practices in micelle studies, where transient water within micelles is typically excluded from concentration calculations [42]. The weight concentrations of micelles are typically calculated using molar concentration and molecular weight, especially when calculating the concentration of micelle-forming surfactants. Although pollen microgels are structurally more complex with a hydrogel shell actively retaining water, this analogy supports our choice to exclude internal water, ensuring consistency in defining particle concentration. By treating pollen microgels as discrete particles in this way, we simplify concentration determinations and facilitate more straightforward comparisons across different particle types, despite the unique swelling dynamics of microgels.

In Case 2, the volume fraction associated with the hollow-shell particles can be estimated as $\varphi = 4\pi R^2 hc$, where R and h are the shell radius and thickness, and c is the conventional concentration of particles. Using e.g. $R = 18$ μm and $h = 0.6$ μm (for 0 h KOH-treated microgel) along with $c = 2.2 \times 10^6$ particles/cm^3 (this corresponds to the net weight concentration of 3 mg/mL at pH 7, assuming that microgel particle was viewed as hollow shells), we obtained that φ is small, especially for other pH values, which means, according to Eq. (1), that the effect of microgel on viscosity might be weak. However, our experiments show a significant increase in viscosity due to the microgel, suggesting that Eq. (2) is more appropriate for analysis.

In our system, changes in pH and KOH treatment impact the swelling behavior of pollen microgel or, more specifically, the diameter and volume of the microparticles (Fig. 4), altering the weight concentration based on the amount of absorbed water even if the conventional net pollen concentration is constant. The corresponding changes of the

microgel viscosity can be interpreted by using Eq. (2). Following this line, we focus on the experiments with constant conventional microgel particle concentration. To employ Eq. (2), we use the weight pollen concentration, c, taking absorbed water into account but excluding water inside shells. This concentration, is below referred to as the effective weight concentration (Fig. S8 and S9) with "effective" added to prevent confusion with the net pollen concentration. In general, higher pH values increased particle diameter, except at pH 11, which subsequently increased the effective weight concentration, implying that the absorbed water during swelling contributed to the increased weight of the microparticles. In fact, the effective weight concentration is associated primarily with water absorbed by the pollen shells.

As usual in applications of Eq. (2), our first step is to determine the intrinsic viscosity, η_{in}, by using the viscosity measured at low c or, more specifically, at $\eta_{in}c \ll 1$ and $(k/\nu)\eta_{in}c \ll 1$. In this limit, the first-order expansion of the exponential function in Eq. (2) yields $exp[\eta_{in}c/(1-(k/\nu)\eta_{in}c)] \simeq 1 + \eta_{in}c$ and accordingly Eq. (2) can be rewritten as

$$\eta \simeq \eta_0(1 + \eta_{in}c), \text{ or } \eta_{in} = \lim_{c\to 0}\left(\frac{\eta - \eta_0}{c\eta_0}\right). \quad (3)$$

Using the latter relation with $\eta_0 = 0.0889$ mPa·s, we have obtained η_{in}= 0.32, 1.90, 8.8, and 5.5 mL/mg for 3, 6, 12, and 24 h KOH-treated microgel samples, respectively. With the specified values of c, η_0, and η_{in} at hand, we have used Eq. (3) to fit the dependence of η on c measured for the samples under consideration (Fig. 8). It was done by employing k/ν as a lumped fitting parameter. For 3 and 6 h KOH-treated samples, the fitting is good provided $k/\nu = 0.47$ and -0.10, respectively (Fig. 8a and b). For 12 and 24 h KOH-treated samples (Fig. 8c and d), η drops at pH 11, and good full-scale fitting is difficult.

For comparison, it is worth mentioning that in the case of protein suspensions k/ν is usually positive (0.45 for BSA in [43], and 0.37–0.49 for hemoglobin [39,44,45]). In our case, the 3 h KOH-treated sample behaves like proteins, whereas the samples with extended KOH treatment alter their swelling behavior in response to pH and KOH-treatment changes, leading to distinct particle-particle interactions compared to proteins or other biological entities such as cells or vesicles, ranging from 10 to 15 mPa·s [46], and up to 102–104 mPa·s under specific conditions [44]. The viscosity of human red blood cells (RBCs) ranges from 4.1 to 23.9 mPa·s at 37 °C, depending on the hemoglobin concentration [47]. Blood plasma viscosity, often used as a model for biological vesicle suspensions, is approximately 1.2 mPa·s [48], while mammalian cell culture suspensions exhibit viscosities ranging from 1 to 105 mPa·s, influenced by cell concentration and applied shear rate [49]. In contrast, pollen microgels demonstrate significantly higher viscosity compared to proteins or cells at higher concentrations associated with pH increase.

3.3. Effect of pH on rheological properties

Initially, at extreme acidic condition at pH 3, 12 h KOH incubated microgels solution was not homogeneous due to the formation of aggregated clusters (Fig. 1d). Agglomeration caused liquid-solid phase separation at pH 3, which decreased elastic properties and increased viscosity significantly, making rheological measurements impossible [50,51]. At pH 5, with increasing angular frequency (0 to 100 rad/s), the

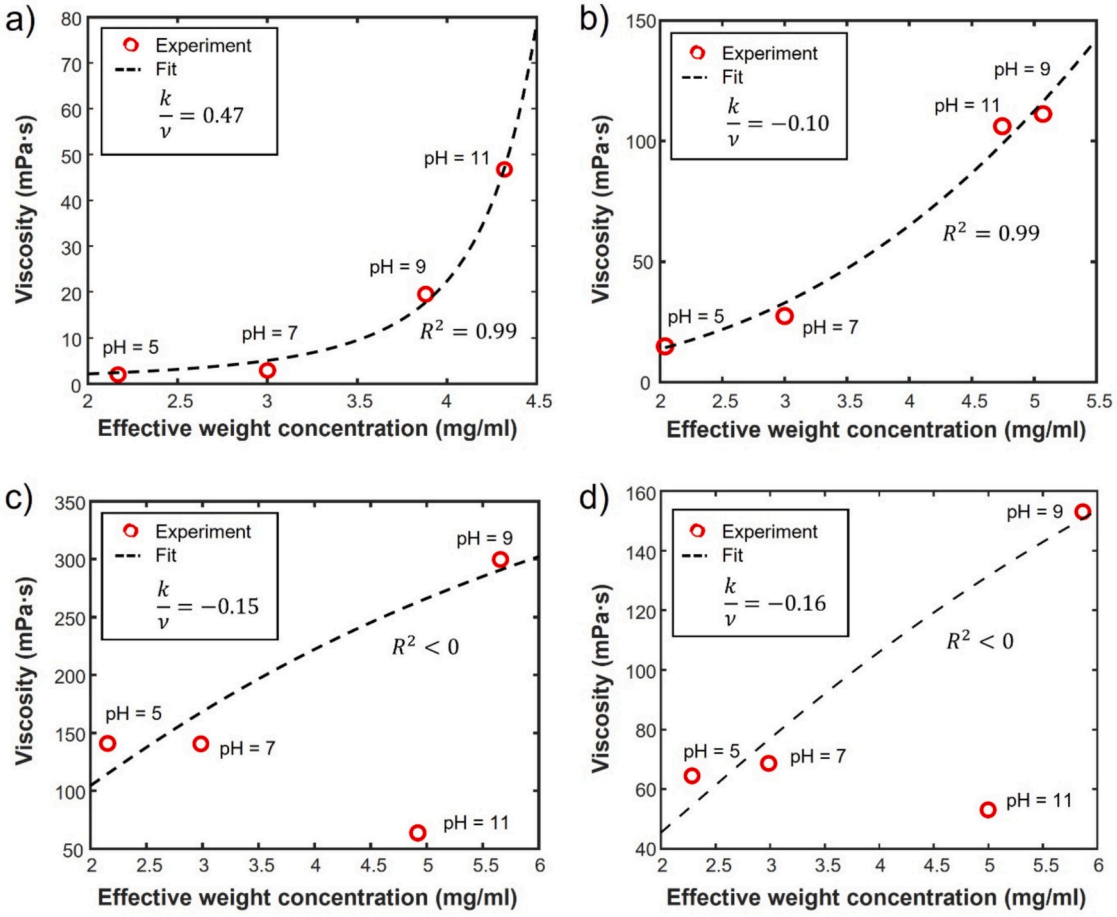

Fig. 8. Viscosity of pollen microgels as a function of the effective weight concentration for different pH conditions (5, 7, 9, and 11) and after prolonged KOH treatment during 3 (a), 6 (b), 12 (c) and 24 h (d). The circles show the data points obtained at 1000 s^{-1}. The dashed lines correspond to Eq. (2), with the lumped fitted parameter k/ν.

loss modulus (G'') increased more rapidly than the storage modulus (G'), and eventually the difference between the two moduli became nearly negligible at high frequency as shown in Fig. 9a. Additionally, the overall storage modulus of pH 5 equilibrated microgel (Fig. 9a) was also significantly lower (49 Pa) than the neutral (133 Pa at pH 7, Fig. 9b) and alkaline conditions (240 Pa at pH 9, Fig. 9c) which reveals the adverse impacts of the acidic condition at pH 5 on the structural stability of the microgel.

Furthermore, as the pH was increased from 7 to 11, the storage modulus (G') exceeded the loss modulus (G'') across a range of frequencies (0.1–100 rad/s). This behavior indicates that the microgel exhibits more solid-like characteristics rather than behaving like a liquid, particularly under alkaline conditions **(**Fig. 9b–d**).** Notably, both G' and G'' exhibit a weak linear dependence on frequency within the pH range of 7–9 (Fig. 9b and c**)**, which is a hallmark of gel-like viscoelastic behavior [52,53]. Moreover, overall loss factor (tan δ) value of the pH 9 equilibrated microgel decreased to ~50 % (0.18) compared to the pH 7 system (0.35) at the maximum angular frequency (100 rad/s), revealing viscoelasticity of the microgel was improved in alkaline condition (**Fig. S5**). Conversely, viscoelastic behavior of the microgels was extensively compromised at the acidic condition (pH 5) due to the higher tan δ (0.63) at the maximum frequency range (100 rad/s) compared to the pH 7–11 conditions (**Fig. S5**) and revealed that the viscoelasticity of microgels was improved under alkaline conditions.

Further pH increase (pH 11) caused a significant reduction in both storage (G') and loss moduli (G''), 30 and 4.0 Pa, respectively, which were significantly lower than the pH 9 system ($G' = 200$ Pa, $G'' = 30$ Pa) across an initial spectrum of frequencies (0.1–35 rad/s) as depicted in Fig. 9c and d. Interestingly, both storage and loss moduli of pH 11 equilibrated microgel were gradually increased at higher oscillation frequency range (50–100 rad/s) (Fig. 9d) and reached almost similar levels identical to pH 9 condition (Fig. 9c). High oscillation frequency can indeed enhance collisions between the solvent K^+ ions and carboxylate ions present in microgel structure and the excess of K^+ ions at pH 11 condition reduced the repulsion between the negative charges of the carboxyl groups more effectively, facilitating strong chain association inside microgel polymeric structure and creating a rigid network structure. Additionally, strong crosslinking between K^+ ions and $–COO^-$ ions allowed the formation of stable gel networks through improved polymeric chain entanglement (Scheme 1), as evidenced by the concurrent rise of both storage and loss moduli in the absence of a crossover point (Fig. 9d).

Additionally, lowest tan δ value (0.14) at the maximum angular frequency (100 rad/s) further supports the improved viscoelasticity of the microgel in adverse condition at pH 11 (**Fig. S5**), making the microgel stiffer and less prone to deformation. However, the concurrent rise of both storage and loss moduli features at pH 11 completely disappeared in the absence of K^+ ions after equilibration of microgels in the presence of CAPS pH 11 buffer (**Fig. S6**), confirming the indispensability of K^+ ions to form cross-linked polymeric network with $–COO^-$ ions present in microgel structure.

In the presentation above, the storage and loss moduli, G' and G'', were introduced axiomatically. To extend the discussion, we recall that in dynamic oscillatory shear measurements the deformation is sinusoidal,

$$\gamma(t) = \gamma_0 sin(\omega t), \tag{4}$$

where γ_o is strain amplitude at given frequency ω [54]. In conventional measurements, the amplitude of the applied strain is considered to be small, and the stress response is represented as

$$\sigma(t) = \gamma_0[G' sin(\omega t) + G'' cos(\omega t)] \tag{5}$$

This expression can be viewed just as a linear expansion. Physically, it can be clarified by using various phenomenological models [55,56]. In particular, the Kelvin-Voigt model is one of the simplest and most

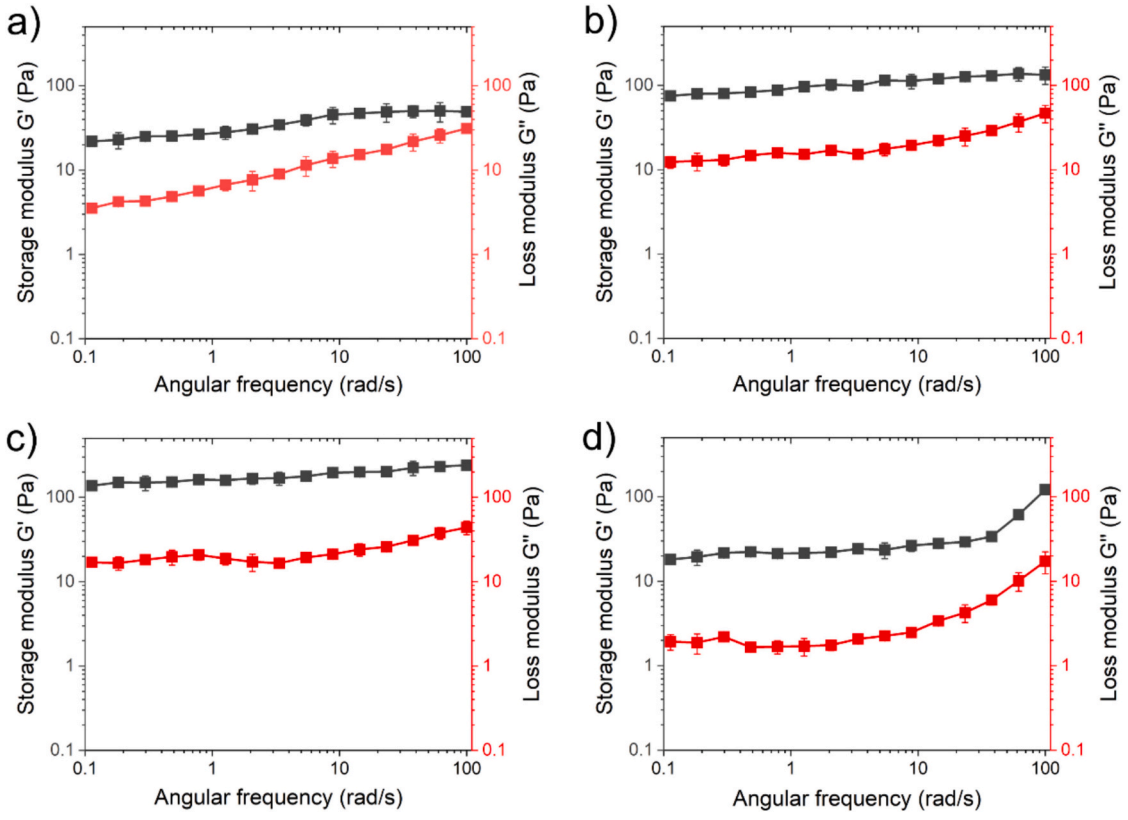

Fig. 9. In a frequency sweep test, storage (G') and loss (G'') moduli of sunflower pollen microgels were determined at different pH conditions, pH 5 (**a**), pH 7 (**b**), pH 9 (**c**), pH 11 (**d**). Error bars represent standard deviation ($n = 3$).

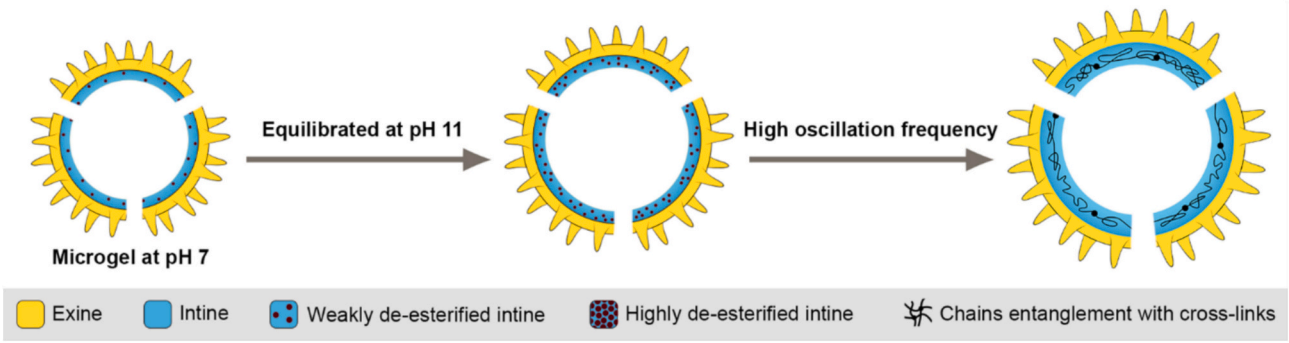

Scheme 1. Diagram of the formation of cross-linked polymeric network inside a microgel particle at high alkaline conditions, pH 11.

popular models in this area [56,57]. According to this model, the stress is expressed via strain as

$$\sigma(t) = \mu\gamma_0 sin(\omega t) + \eta\gamma_0\omega cos(\omega t), \quad (6)$$

where μ is the elastic shear modulus, and η is the share viscosity. Comparing eqs. (5) and (6) yields $G' = \mu$ and $G'' = \omega\eta$. These relations are instructive from various perspective. For example, one general consequences of the proportionality of G'' to ω is that G'' increases faster than G' with increasing ω. Another general remark is that the Kelvin-Voigt model is sometimes employed in the QCM-D measurements [58–61], and from this perspective, eqs. (5) and (6) allow one to link the rheological and QCM-D data.

4. Conclusions

In the present work, we have established in detail the pH-responsive structural alteration of pollen microgels and filled the gap between the characterization of microgels in the bulk colloidal solution and at the single particle level. The pH-dependent swelling dynamics of pollen microgels and their effects on bulk rheology and local elastic properties were experimentally examined and theoretically interpreted using the Ross-Minton equation for suspension viscosity. This analysis revealed unique particle interactions in pollen microgels, distinct from those in proteins or other biological particles. Also, the present findings uncover that, although pollen microgels have extensively been studied for a last decade, there is still significant untouched areas. In particular, the altering rheological characteristics or tuneable viscoelasticity (compressibility and deformability) of the pollen microgels at high alkaline condition (e.g. pH 11), allows one to manipulate its spherical shapes so that microgel particles form a densely packed structure which could have enormous potential in many applications, including 3D material or printing technology, biomedical applications (e.g. wound dressing, drug delivery vehicles and tissue regeneration), agriculture (e.g. wastewater treatment), and superhydrophobic biolubricant. With the reservation above, several limitations should be acknowledged. First, while we demonstrated pH-responsive swelling and its impact on rheological properties, the long-term stability of these microgels under repeated pH cycles remains unexplored. Additionally, this study primarily focused on sunflower pollen microgels, and further investigations are needed to assess whether similar behaviors occur in other pollen species with varying structural and chemical compositions. Finally, while we discussed the potential for external stimuli such as chelating agents (e.g., EDTA) and electrolyte concentration changes to influence pollen microgel behavior, a detailed mechanistic study is still required to fully understand these effects. Addressing these limitations in future research will provide a more comprehensive understanding of pollen microgels and enable their precise tuning for targeted applications in drug delivery, biosensing, sustainable coatings, and soft material engineering.

CRediT authorship contribution statement

Snehasish Basu: Writing – review & editing, Writing – original draft, Visualization, Validation, Methodology, Investigation, Formal analysis, Data curation, Conceptualization. **Mohammed Shahrudin Bin Ibrahim:** Writing – original draft, Validation, Methodology, Formal analysis, Data curation. **Jian Li:** Methodology. **Jueying Yang:** Methodology. **Ahmad Albar:** Visualization. **Abdul Rahim Ferhan:** Writing – review & editing. **Vladimir P. Zhdanov:** Writing – review & editing, Formal analysis, Conceptualization. **Du Yeol Ryu:** Writing – review & editing, Funding acquisition, Formal analysis. **Nam-Joon Cho:** Writing – review & editing, Writing – original draft, Validation, Resources, Funding acquisition, Formal analysis, Conceptualization. **Juha Song:** Writing – review & editing, Project administration, Funding acquisition, Conceptualization. **Woncheol Jeong:** Writing – review & editing, Writing – original draft, Validation, Formal analysis.

Declaration of competing interest

The authors declare the following financial interests/personal relationships which may be considered as potential competing interests: Dr. Juha Song reports that the financial support was provided by Government of Singapore Ministry of Education. Dr. Nam-Joon Cho reports that the financial supports were provided by National Research Foundation, Singapore and Yonsei University, South Korea. The other authors declare that they have no known competing financial interests or personal relationships that could have appeared to influence the work reported in this paper. Dr. Juha Song is an Associate Editor for this journal and was not involved in the editorial review or the decision to publish this article.

Acknowledgments

This work was supported by the Nanyang Technological University, Singapore via its characterization user facilities, Ministry of Education (MOE, Singapore) Academic Research Fund Tier3 2022 under Award Number MOE-MOET32022-0002. This research was also supported by the National Research Foundation, Prime Minister's Office, Singapore under its Campus for Research Excellence and Technological Enterprise

(CREATE) programme through the funding provided to the programme titled CellAg (Award Number: REQ414940): Bioengineering Tools for Next-Generation Cellular Agriculture. Dr. NJ Cho acknowledges the support provided by the Yonsei University Research Fund (Yonsei Frontier Lab, Yonsei Frontier Program for Outstanding Scholars).

Appendix A. Supplementary data

Supplementary data to this article can be found online at https://doi.org/10.1016/j.bioadv.2025.214231.

Data availability

Data will be made available on request.

References

[1] J.M. Tylianakis, The global plight of pollinators, Science 339 (2013) 1532–1533.
[2] W.E. Friedman, Sexual reproduction in Ephedra nevadensis (Ephedraceae): further evidence of double fertilization in a nonflowering seed plant, Am. J. Bot. 77 (1990) 1582–1598.
[3] J.G. Rodger, J.M. Bennett, M. Razanajatovo, T.M. Knight, M. van Kleunen, T.-L. Ashman, J.A. Steets, C. Hui, G. Arceo-Gómez, M. Burd, Widespread vulnerability of flowering plant seed production to pollinator declines, Sci. Adv. 7 (2021) eabd3524.
[4] A. Diego-Taboada, P. Cousson, E. Raynaud, Y. Huang, M. Lorch, B.P. Binks, Y. Queneau, A.N. Boa, S.L. Atkin, S.T. Beckett, Sequestration of edible oil from emulsions using new single and double layered microcapsules from plant spores, J. Mater. Chem. 22 (2012) 9767–9773.
[5] G. Mackenzie, A.N. Boa, A. Diego-Taboada, S.L. Atkin, T. Sathyapalan, Sporopollenin, the least known yet toughest natural biopolymer, Front. Mater. 2 (2015) 66.
[6] H.J.B. Birks, H.H. Birks, B. Ammann, The fourth dimension of vegetation, Science 354 (2016) 412–413.
[7] X. Ma, Y. Wu, G. Zhang, Formation pattern and regulatory mechanisms of pollen wall in Arabidopsis, J. Plant Physiol. 260 (2021) 153388.
[8] Z. Qu, J.C. Meredith, The atypically high modulus of pollen exine, J. R. Soc. Interface 15 (2018) 20180533.
[9] Z. Zhao, J. Deng, H. Tae, M.S. Ibrahim, S. Suresh, N. Cho, Recyclable and reusable natural plant-based paper for repeated digital printing and Unprinting, Adv. Mater. 34 (2022) 2109367.
[10] S. Chen, Q. Shi, T. Jang, M.S.B. Ibrahim, J. Deng, G. Ferracci, W.S. Tan, N.-J. Cho, J. Song, Engineering natural pollen grains as multifunctional 3D printing materials, Adv. Funct. Mater. 31 (2021) 2106276, https://doi.org/10.1002/adfm.202106276.
[11] C.C. Mayorga-Martinez, M. Fojtů, J. Vyskočil, N. Cho, M. Pumera, Pollen-based magnetic microrobots are mediated by electrostatic forces to attract, manipulate, and kill Cancer cells, Adv. Funct. Mater. 32 (2022) 2207272.
[12] Y. Hwang, M.K. Kim, Z. Zhao, B. Kim, T. Chang, T.F. Fan, M.S. Ibrahim, S. Suresh, C.H. Lee, N.-J. Cho, Plant-based substrate materials for flexible green electronics, Adv. Mater. Technol. 7 (2022) 2200446, https://doi.org/10.1002/admt.202200446.
[13] J. Kim, J. Deng, N. Cho, S.M. Han, Directional, Silanized plant-based sponge for oil collection, Adv. Funct. Mater. 2313808 (2024).
[14] J. Deng, Z. Zhao, X.Y. Yeo, C. Yang, J. Yang, A.R. Ferhan, B. Jin, C. Oh, S. Jung, S. Suresh, Plant-based shape memory cryogel for hemorrhage control, Adv. Mater. 36 (2024) 2311684.
[15] Q. Shi, M.S.B. Ibrahim, X. Zhang, Y. Hwang, H. Chin, S. Chen, W.S. Tan, H. Li, J. Song, N.-J. Cho, Unraveling the distinct germination processes of sporopollenin-based pollen grains and spores through morphological analyses upon natural nano-architectonics process, Appl. Mater. Today 27 (2022) 101471.
[16] R. Gentili, R. Ambrosini, C. Montagnani, S. Caronni, S. Citterio, Effect of soil pH on the growth, reproductive investment and pollen allergenicity of Ambrosia artemisiifolia L, Front. Plant Sci. 9 (2018) 1335.
[17] L. Fan, Y. Wang, H. Wang, W. Wu, In vitro Arabidopsis pollen germination and characterization of the inward potassium currents in Arabidopsis pollen grain protoplasts, J. Exp. Bot. 52 (2001) 1603–1614.
[18] J.K. Pittman, Multiple transport pathways for mediating intracellular pH homeostasis: the contribution of H+/ion exchangers, Front. Plant Sci. 3 (2012) 11.
[19] M. Bosch, P.K. Hepler, Pectin methylesterases and pectin dynamics in pollen tubes, Plant Cell 17 (2005) 3219–3226.
[20] R.D. Hoffmann, M.T. Portes, L.I. Olsen, D.S.C. Damineli, M. Hayashi, C.O. Nunes, J. T. Pedersen, P.T. Lima, C. Campos, J.A. Feijó, Plasma membrane H+-ATPases sustain pollen tube growth and fertilization, Nat. Commun. 11 (2020) 2395.
[21] Z. Lončarić, K. Karalić, B. Popović, D. Rastija, M. Vukobratović, Total and plant available micronutrients in acidic and calcareous soils in Croatia, Cereal Res. Commun. 36 (2008) 331–334.
[22] K.A. Wilkins, M. Bosch, T. Haque, N. Teng, N.S. Poulter, V.E. Franklin-Tong, Self-incompatibility-induced programmed cell death in field poppy pollen involves dramatic acidification of the incompatible pollen tube cytosol, Plant Physiol. 167 (2015) 766–779.
[23] S. Padmanaban, D.D. Czerny, K.A. Levin, A.R. Leydon, R.T. Su, T.K. Maugel, Y. Zou, S. Chanroj, A.Y. Cheung, M.A. Johnson, Transporters involved in pH and K + homeostasis affect pollen wall formation, male fertility, and embryo development, J. Exp. Bot. 68 (2017) 3165–3178.
[24] F.W. Gibbs, The history of the manufacture of soap, Ann. Sci. 4 (1939) 169–190.
[25] T.-F. Fan, S. Park, Q. Shi, X. Zhang, Q. Liu, Y. Song, H. Chin, M.S.B. Ibrahim, N. Mokrzecka, Y. Yang, Transformation of hard pollen into soft matter, Nat. Commun. 11 (2020) 1449.
[26] G.H. Pollack, Cells, Gels and the Engines of Life: A New, Unifying Approach to Cell Function, Ebner & Sons Seattle, WA, 2001.
[27] D.J. Beebe, J.S. Moore, J.M. Bauer, Q. Yu, R.H. Liu, C. Devadoss, B.-H. Jo, Functional hydrogel structures for autonomous flow control inside microfluidic channels, Nature 404 (2000) 588–590.
[28] T. Fan, Y. Hwang, M.S. Ibrahim, G. Ferracci, N.-J. Cho, Influence of chemical and physical change of pollen microgels on swelling/De-swelling behavior, Macromol. Rapid Commun. 41 (2020) 2000155.
[29] E. Parre, A. Geitmann, Pectin and the role of the physical properties of the cell wall in pollen tube growth of Solanum chacoense, Planta 220 (2005) 582–592.
[30] J.B. Wehr, N. Menzies, F. Blamey, Alkali hydroxide-induced gelation of pectin, Food Hydrocoll. 18 (2004) 375–378.
[31] M.-A. Bornik, L.W. Kroh, D-Galacturonic acid as a highly reactive compound in nonenzymatic browning. 1. Formation of browning active degradation products, J. Agric. Food Chem. 61 (2013) 3494–3500.
[32] D. Oakenfull, A. Scott, Hydrophobic interaction in the gelation of high methoxyl pectins, J. Food Sci. 49 (1984) 1093–1098.
[33] M.L. Fishman, P.H. Cooke, H.K. Chau, D.R. Coffin, A.T. Hotchkiss, Global structures of high methoxyl pectin from solution and in gels, Biomacromolecules 8 (2007) 573–578.
[34] C. Lara-Espinoza, E. Carvajal-Millán, R. Balandrán-Quintana, Y. López-Franco, A. Rascón-Chu, Pectin and pectin-based composite materials: beyond food texture, Molecules 23 (2018) 942.
[35] C. Löfgren, A.-M. Hermansson, Synergistic rheological behaviour of mixed HM/LM pectin gels, Food Hydrocoll. 21 (2007) 480–486.
[36] L. Flutto, PECTIN | properties and determination, in: B. Caballero (Ed.), Encycl. Food Sci. Nutr, Second ed., Academic Press, Oxford, 2003, pp. 4440–4449, https://doi.org/10.1016/B0-12-227055-X/00901-9.
[37] L.D. Landau, E.M. Lifshitz, Fluid Mechanics, Elsevier, Amsterdam, 1987.
[38] M.A. Rahman, S.M. Hasnain, S. Pandey, A. Tapalova, N. Akylbekov, R. Zairov, Review on nanofluids: preparation, properties, stability, and thermal performance augmentation in heat transfer applications, ACS Omega 9 (2024) 32328–32349.
[39] P.D. Ross, A.P. Minton, Hard quasispherical model for the viscosity of hemoglobin solutions, Biochem. Biophys. Res. Commun. 76 (1977) 971–976.
[40] F. Otto, F. Dallari, F. Westermeier, D.F. Wieland, W.J. Parak, F. Lehmkühler, F. Schulz, The dynamics of PEG-coated nanoparticles in concentrated protein solutions up to the molecular crowding range, Aggregate 5 (2024) e483.
[41] C.M. Lewis, C.T. Heise, N. Harasimiuk, J. Tovey, J.R. Lu, T.A. Waigh, The viscoelasticity of high concentration monoclonal antibodies using particle tracking microrheology, APL Bioeng. 8 (2024).
[42] M.J. Rosen, J.T. Kunjappu, Surfactants and Interfacial Phenomena, John Wiley & Sons, 2012.
[43] S. Yadav, S.J. Shire, D.S. Kalonia, Viscosity analysis of high concentration bovine serum albumin aqueous solutions, Pharm. Res. 28 (2011) 1973–1983.
[44] M.R. Alizadehfard, D.E. Wiley, Viscosity of whey protein solutions, Iran. J. Polymer Sci. Technol. 4 (1995).
[45] S. Kanai, J. Liu, T.W. Patapoff, S.J. Shire, Reversible self-association of a concentrated monoclonal antibody solution mediated by Fab–Fab interaction that impacts solution viscosity, J. Pharm. Sci. 97 (2008) 4219–4227, https://doi.org/10.1002/jps.21322.
[46] M. Zidar, P. Rozman, K. Belko-Parkel, M. Ravnik, Control of viscosity in biopharmaceutical protein formulations, J. Colloid Interface Sci. 580 (2020) 308–317.
[47] A. Rezghi, J. Zhang, Tank-treading dynamics of red blood cells in shear flow: on the membrane viscosity rheology, Biophys. J. 121 (2022) 3393–3410.
[48] D. Božič, S. Sitar, I. Junkar, R. Štukelj, M. Pajnič, E. Žagar, V. Kralj-Iglič, K. Kogej, Viscosity of plasma as a key factor in assessment of extracellular vesicles by light scattering, Cells 8 (2019) 1046.
[49] Y. Shi, D.D. Ryu, R. Ballica, Rheological properties of mammalian cell culture suspensions: Hybridoma and HeLa cell lines, Biotechnol. Bioeng. 41 (1993) 745–754.
[50] S. Khan, V. Kumar, P. Roy, P.P. Kundu, TiO 2 doped chitosan/hydroxyapatite/halloysite nanotube membranes with enhanced mechanical properties and osteoblast-like cell response for application in bone tissue engineering, RSC Adv. 9 (2019) 39768–39779.
[51] S. von Bülow, M. Siggel, M. Linke, G. Hummer, Dynamic cluster formation determines viscosity and diffusion in dense protein solutions, Proc. Natl. Acad. Sci. 116 (2019) 9843–9852.
[52] M. Bertasa, A. Dodero, M. Alloisio, S. Vicini, C. Riedo, A. Sansonetti, D. Scalarone, M. Castellano, Agar gel strength: a correlation study between chemical composition and rheological properties, Eur. Polym. J. 123 (2020) 109442.
[53] A. Charisis, E.P. Kalogianni, Alginate-chitosan microgel particles, water–oil interfacial layers, and emulsion stabilization, Coll. Interf. 7 (2023) 48.
[54] M.Y. Erturk, A.N.M. Le, J. Kokini, Advances in large amplitude oscillatory shear rheology of food materials, Front. Food Sci. Technol. 3 (2023) 1130165.
[55] S.S. Poul, J. Ormachea, R.G. Gary, K.J. Parker, Comprehensive experimental assessments of rheological models' performance in elastography of soft tissues, Acta Biomater. 146 (2022) 259–273.

[56] M. Osika, P. Kijanka, Ultrasound shear wave propagation modeling in general tissue–like viscoelastic materials, Ultrasound Med. Biol. 50 (2024) 627–638.
[57] A. Mishra, R.O. Cleveland, Rheological properties of porcine organs: measurements and fractional viscoelastic model, Front. Bioeng. Biotechnol. 12 (2024) 1386955.
[58] M.V. Voinova, M. Rodahl, M. Jonson, B. Kasemo, Viscoelastic acoustic response of layered polymer films at fluid-solid interfaces: continuum mechanics approach, Phys. Scr. 59 (1999) 391.
[59] N.-J. Cho, K.K. Kanazawa, J.S. Glenn, C.W. Frank, Employing two different quartz crystal microbalance models to study changes in viscoelastic behavior upon transformation of lipid vesicles to a bilayer on a gold surface, Anal. Chem. 79 (2007) 7027–7035.
[60] S.R. Tabaei, J.J. Gillissen, N.-J. Cho, Probing membrane viscosity and interleaflet friction of supported lipid bilayers by tracking electrostatically adsorbed, nano-sized vesicles, Small 12 (2016) 6338–6344.
[61] S.R. Tabaei, J.J. Gillissen, M.C. Kim, J.C. Ho, B. Liedberg, A.N. Parikh, N.-J. Cho, Brownian dynamics of electrostatically adhering small vesicles to a membrane surface induces domains and probes viscosity, Langmuir 32 (2016) 5445–5450.